Journal of Molecular Graphics and Modelling 45 (2013) 1–12

Contents lists available at ScienceDirect

Journal of Molecular Graphics and Modelling

journal homepage: www.elsevier.com/locate/JMGM

Molecular modeling and simulation of FabG, an enzyme involved in the fatty acid pathway of *Streptococcus pyogenes*

Rajamohmed Beema Shafreen, Shunmugiah Karutha Pandian*

Department of Biotechnology, Alagappa University, Karaikudi, Tamil Nadu, India

ARTICLE INFO

Article history:
Received 13 March 2013
Received in revised form 28 July 2013
Accepted 30 July 2013
Available online 13 August 2013

Keywords:
FabG (β-Ketoacyl Carrier Protein Reductase)
Streptococcus pyogenes
Homology modeling
ADMET
Cerulenin
Epigallocatechin

ABSTRACT

Streptococcus pyogenes (SP) is the major cause of pharyngitis accompanied by strep throat infections in humans. 3-keto acyl reductase (FabG), an important enzyme involved in the elongation cycle of the fatty acid pathway of *S. pyogenes*, is essential for synthesis of the cell-membrane, virulence factors and quorum sensing-related mechanisms. Targeting SPFabG may provide an important aid for the development of drugs against *S. pyogenes*. However, the absence of a crystal structure for FabG of *S. pyogenes* limits the development of structure-based drug designs. Hence, in the present study, a homology model of FabG was generated using the X-ray crystallographic structure of *Aquifex aeolicus* (PDB ID: 2PNF). The modeled structure was refined using energy minimization. Furthermore, active sites were predicted, and a large dataset of compounds was screened against SPFabG. The ligands were docked using the LigandFit module that is available from Discovery Studio version 2.5. From this list, 13 best hit ligands were chosen based on the docking score and binding energy. All of the 13 ligands were screened for Absorption, Distribution, Metabolism, Excretion and Toxicity (ADMET) properties. From this, the two best descriptors, along with one descriptor that lay outside the ADMET plot, were selected for molecular dynamic (MD) simulation. *In vitro* testing of the ligands using biological assays further substantiated the efficacy of the ligands that were screened based on the *in silico* methods.

1. Introduction

Streptococcus pyogenes is a gram-positive, non-motile, spherical bacterium. It is responsible for various human diseases, ranging from trivial to lethal [1]. Although penicillin is the drug of choice for the treatment of *S. pyogenes* infections, macrolides are used for patients who are allergic to β-lactams. The emergence of macrolide resistance in *S. pyogenes* is an increasing problem worldwide [2,3]. Furthermore, the indiscriminate usage of synthetic antimicrobials to treat infections caused by macrolide-resistant *S. pyogenes* has resulted in a strain that has multiple resistances to a major class of antibiotics [4]. In addition, the high cost and adverse side effects (*e.g.*, hypersensitivity, allergic reactions and immunosuppression) of the synthetic antimicrobials used for treating infectious diseases are major issues [5]. Today, there is an urgent and continuous need to identify compounds that are biologically active and incur minimal side effects.

Antibiotics of plant origin have vast therapeutic potential. They have proven effective when used for treatment against infectious diseases, simultaneously extenuating many of the side effects associated with synthetic antimicrobials [6]. The positive effect of potential antimicrobials from natural products with few or no side effects might depend on the structure of the compound that interacts with the toxin or pathogen and not with other molecules in the physiology of the host. This approach has become the rationale for drug design studies as a new field of research.

An extensive literature survey suggests that consuming tea (*Camellia sinensis* L.) enhances the immune system capacity to fight infectious diseases [7–9]. Important micronutrients, vitamins and minerals that are present in green tea produce its free radical capturing (antioxidant), invigorating (caffeine) and detoxifying antibacterial properties. Although the detailed mechanism of the antimicrobial activity of catechins present in green tea remains unexplored, the common target of catechins is the cell membrane of the pathogen (with broad-spectrum activity), in addition to specific targets for each pathogen [10].

Type II FAS pathway was previously reported as a significant antimicrobial target [11,12]. Findings of Brinster and Balemans [13] have opened up a demanded debate, whether FAS II pathway is suitable drug target. Furthermore, targeting FAS II pathway varies, even though the bacteria are closely related to each other. Researchers have well demonstrated that FAS II enzymes may not be suitable target during intraperitoneal infection caused by *Streptococcus agalactiae*, but these enzymes might be suitable target for eradication of cutaneous antibiotic-resistant bacteria involved in

* Corresponding author at: Department of Biotechnology, Alagappa University, Karaikudi 630 003, Tamil Nadu, India. Tel.: +91 4565 225215; fax: +91 4565 229334.
E-mail address: sk_pandian@rediffmail.com (S.K. Pandian).

1093-3263/$ – see front matter © 2013 Elsevier Inc. All rights reserved.
http://dx.doi.org/10.1016/j.jmgm.2013.07.009

cutaneous infection [14]. Additionally, bacterial FAS II pathway is a desirable for drug discovery because the pathway is not targeted by existing drugs and is therefore likely to produce compounds that inhibit the bacteria which show resistance to the known antibiotics [15]. Recently, FabK of *Streptococcus pneumoniae* is described as an attractive and potential target for developing selective antibacterial agents [16,17]. Based on these highlights, identification of antimicrobial agents against FAS II pathway of *S. pyogenes* was chosen as desirable target for the present study. The *fabG* gene product, β-ketoacyl-acyl carrier protein (ACP) reductase (FabG), plays a key role in the synthesis of fatty acids [18]. FabG is highly conserved and ubiquitously expressed in all bacteria and is the only known isozyme that catalyzes the essential ketoreduction steps in the elongation cycle of FAS II [19–21]. Therefore, FabG represents a valid target that is yet to be explored for the development of broad-spectrum antimicrobial agents. The elongation-condensing enzymes play an important role in the regulation of fatty acid biosynthesis; because natural products are known to target this step in the pathway, FabG is clearly a desirable target for therapeutics development [22].

Natural compounds such as epigallocatechin gallate (EGCG; *e.g.*, green tea catechin) and C-3 gallic acid esters of the catechins have been reported to be potent inhibitors of FabG in *Escherichia coli* and *Plasmodium falciparum* [21,23]. To date, inhibitors against FabG of *S. pyogenes* have not been explored. As a prelude to such exploration, a three-dimensional (3D) homology model of FabG from *S. pyogenes* was developed, and a large dataset of compounds was screened against the model. The compounds screened (based on the structure-based virtual screening) were experimentally tested using biological assays.

2. Materials and methods

2.1. Homology modeling

The FabG protein sequence of *S. pyogenes* (ACZ64265) was retrieved from the NCBI database, and a basic local alignment search tool (BLAST) [24] analysis for the enzyme (FabG) was performed against the protein data bank (PDB) [25] using the default parameters to find a suitable template for homology modeling. Based on the maximum identity with a high score and low *e*-value, PDB ID: 2PNF (from *Aquifex aeolicus*) at a resolution of 1.8 Å was selected as the most appropriate template for homology modeling [26]. The sequence alignment between the target and the template was calculated using the DS Modeler, module from Discovery Studio 2.5 program, distributed by Accelrys Software Inc., San Diego, CA, USA [27]. Further energy minimization was performed using DS CHARMm to remove the geometric restraints of the SPFabG model. The secondary structure of the model was analyzed using PDBsum (available from http://www.ebi.ac.uk/pdbsum). On the SAVES server, Ramachandran's map was drawn using PROCHECK v.3.0, and non-bonded interactions between different atom types were calculated using ERRAT graph. The refined structure was chosen for further study.

2.2. Binding pocket identification

The "Define and edit binding site" protocol in Discovery Studio was used to identify the potential binding site in the protein [28]. A ligand-based search strategy was also applied, in which the known ligand (NADPH) binding active site is defined as the binding pocket for the other test ligands. Based on the earlier report of Miller et al. [29], a detailed comparison of structures from *Pseudomonas aeruginosa* (RhlG) and *E. coli* (FabG) indicated three active site residues (Ser, Tyr, and Lys) with identical roles in catalysis. The multiple sequence alignment of the FabG sequences (*P. aeruginosa*, *E. coli*, *Staphylococcus aureus*, *A. aeolicus* and *S. pyogenes*) showed highly conserved active site residues in FabG of *S. pyogenes*. This identification has assisted in locating the exact binding site in the homology model of *S. pyogenes.*

2.3. Ligand database generation and molecular docking

ACD/ChemSketch an integrated software package from Advanced Chemistry Development Inc. was used for drawing the chemical structure of CID 65064 (Epigallocatechin gallate (EGCG)). The 3D optimization algorithm in ChemSketch was used to rapidly translate the 2D planar structure into a sensible 3D structure. The 3D optimization algorithm based on CHARMM force field was applied to optimize the ligand. The 3D structure of EGCG was used as a search key against PubChem, a database of chemical and small molecule structures. The search key retrieved a series of chemical substructure with the similarity percentage of 80% and the Tanimoto score of >0.9 representing the increased possibility of these selected substructure with same bioactivity. The search resulted in 60,485 similar structures were used as library for virtual screening (VS).

Prior to VS, the homology model (SPFabG) and the library of compounds was minimized to their low energy state using the CHARMm force field implemented in DS 2.5. The convergence gradient was set to 0.01 kcal mol^{-1}, and 10,000 steps of a steepest descent algorithm were performed following 50,000 steps of conjugate gradient algorithm. A spherical cut-off of 14 Å was used for non-bonding interactions, and the other parameters were set to their default values. To validate the docking protocol setup prior to screening, the known inhibitor CID: 65064 was docked in the ligand-binding site, and the results were compared with earlier output. Then, the database was subjected to virtual screening against the homology model. The LigandFit module in DS 2.5 was used for docking the compound database. The LigandFit docking procedure follows two major elements: (i) defining the binding sites of the receptor specific for docking and (ii) docking the ligands to the specified site [30]. The top 10 docked poses were allowed to be saved. The successful poses were evaluated using a set of scoring functions, such as LigScore1, LigScore2, PLP1 and PLP2 were implemented in the DS 2.5 program. The ligands in the binding site were prioritized according to the Dock-Score function. The binding free energies ($\Delta G_{binding}$) of protein–ligand complexes were calculated [31] using the following equation:

$$\Delta G_{binding} = \Delta G_{complex} - \Delta G_{drug} - \Delta G_{target} \quad (1)$$

The top 10 poses obtained after docking were used for calculating the binding energies.

2.4. ADMET prediction

The ADMET descriptor describes the kinetics of drug exposure to tissue and pharmacological activity of the compounds. The ADMET program available in DS 2.5 requires 2D or 3D molecular structure information in either SDF or MOL file formats. The program parses the structure and calculates the values of molecular descriptors. The four ADMET properties were tested for the ligands; the human intestinal absorption descriptor illustrates the absorption of the orally administered drugs in the intestine. The compounds classified based on the predicted values such as "0", "1" and "2" are defined with good, moderate and low absorption respectively. The blood–brain barrier defines the penetration of molecules after oral administration. The cutoff value of "0", "1", "2" and "3" defines very high, high, moderate and low penetration of the compounds. The cytochrome P450 2D6 inhibition predicts the inhibition of the enzyme using 2D chemical structure as an input. The probability

estimate value as "0" defines the compound is not an inhibitor and the value of "1" refers the molecule is an inhibitor. The hepatotoxicity models show the compounds with the value of "0" refers to be non toxic and "1" represents the compounds are toxic [32].

2.5. Molecular dynamics (MD)

MD simulations and analysis were performed using the GROMACS 4.5.5 program for the apo and holo forms. The initial structures of the receptor and ligands were cleaned using the GROMOS96 force field, and the topology files were then generated separately for the receptor and ligands using the PRODRG tool [33]. The simulation system was created manually by importing the ligand topology into the pursued system with a dodecahedron box with a margin of 1 nm, and the system was filled with water using the SPC explicit solvation model. The system was applied with energy minimization, and the atomic velocities were adjusted according to the Maxwell–Boltzmann distribution at 300 K with a periodic scaling of 0.1 ps. A pre-simulation run of 20 ps was applied to relax the system and to remove the geometric restraints, which eventually appeared at the initialization of the run [34]. For equilibration of the apo and holo forms 1000 steps of steepest descent energy minimization and 1000 steps of conjugated gradient energy minimization was carried out in the hybrid water system. Initially the temperature was adjusted with a simple simulation run of 1200 ps annealing from 200 K to 300 K and 200 ps of NVT (number of particles (N), system volume (V), temperature (T) constant) condition [35]. The density adjustment was carried out with the initial run of 500 ps of NPT. The equilibrated structure was further subjected to 10 ns of NpT production dynamic at the temperature of 310 K and 1 bar of pressure. Frames of trajectory were captured at each 4.8 ps time step. The RMSD of the backbone was calculated through the simulation with the first frame as a reference. The RMSD and RMSF results in the initial and final conformations from both the apo and holo forms were incorporated into the results.

2.6. Binding energy calculation

The binding energy calculation was performed to verify the docking results from LigandFit module in DS 2.5. The binding energy calculation was performed for both conformation obtained before and after dynamics using the prime MM/GBSA module from Schrodinger V9.2 LLC, New York, NY 2011. Binding free energies were calculated with the following equations. $\Delta E = E_{complex} - E_{protein} - E_{ligand}$ ($E_{complex}$, $E_{protein}$, and E_{ligand} are the minimized energies of the protein–inhibitor complex, protein and inhibitor respectively). Prime module uses the surface generalized born model which applies a Gaussian surface instead of a vdW surface for enhanced representation of the solvent-accessible surface area [36].

2.7. Antimicrobial activity test

The antimicrobial activity of the inhibitors was assayed by the disk diffusion susceptibility test [Clinical and Laboratory Standards Institute (CLSI), 2006]. The disk diffusion test was performed in Muller–Hinton agar (MHA) (Himedia Laboratories) supplemented with 5% sheep blood. From the overnight culture of *S. pyogenes*, a 3 h subculture was prepared using Todd–Hewitt Broth (THB) until a turbidity of 0.5 McFarland (1×10^8 CFU mL^{-1}) was reached. The lowest concentration of the compounds that concealed the visible growth of *S. pyogenes* was documented as the minimum inhibitory concentration (MIC) [37].

2.8. Preparations of cell extracts

The enzyme used for fatty acid synthesis was isolated according to the method of Heath and Rock [38,39]. *S. pyogenes* was cultured in 500 mL of THB and grown to late log phase. The cultures were centrifuged, and the cells were resuspended in 5 mL of lysis buffer (0.1 M sodium phosphate (pH 7.0), 5 mM Mercaptoethanol, 1 mM EDTA) and lysed at 18,000 lb/in^2. The lysate was centrifuged at 13,400 rpm for 1 h at 4 °C to remove cell debris. The supernatant was saturated to 45% by adding ammonium sulfate, and the precipitated protein was removed by centrifugation for 30 min at 9300 × *g*. Furthermore, the supernatant was saturated to 80% by the addition of ammonium sulfate, and the precipitated protein was collected by centrifugation. The protein pellet was dissolved in 2 mL of lysis buffer and dialyzed for 5 h at 4 °C against 2 L of the same buffer. Protein concentrations were determined using the Bradford assay [40] with bovine serum albumin as the standard.

2.9. Assay of β-ketoacyl–ACP reductase activity

FabG catalyzes the reduction of acetoacetyl-CoA in the presence of the co-enzyme NADPH. The reaction was followed spectrophotometrically by measuring the NADPH concentrations at 340 nm ($\varepsilon 340 = 6.3 \times 10^3$ mol^{-1}). The assay was conducted at room temperature, as described by Toomey et al. [41]. The reaction mixtures contained 0.1 M sodium phosphate at pH 7.0, 1 mM 2-mercaptoethanol, 239 μM NADPH, 58.7 μM acetoacetyl-CoA and 40 μL of crude protein, and the final volume was increased to 3 mL using MilliQ. The inhibition of FabG was tested against different compounds (CER, EGC and EUG). The values from the inhibition assays were first normalized using the negative control (without acetoacetyl-CoA). The percent inhibition and rate of NADPH oxidation was calculated using the formula: [(control − test)/control] × 100. Furthermore, the IC_{50} value showing 50% inhibition was calculated using probit. For which the various concentration of the compounds (0.2–3000 μg/ml) were used for the analysis [42].

2.10. Fluorescence spectroscopy

Fluorescence measurement of the binding assay was carried out to determine the binding affinities of the cofactors to the apoenzymes in the presence and absence of the inhibitors. All the experiments were performed at room temperature using a spectrofluorimeter (Cary Eclipse; Varian) with a quartz cuvette. The assay mixtures were prepared freshly before each set of wavelength scan. The reaction mixture of binding assay includes 239 μM of NADPH, 58.7 μM of acetoacetyl-CoA, 40 μL of crude protein and varying concentrations of the compounds (EGC, CER and EUG). Initially the enzyme-bound to NADPH without the ligands was recorded at 250 to 350 nm excitation wavelength through a 5 nm slit width and the fluorescence emission spectra was recorded from 300 to 500 nm *via* 10 nm slit width. The sample spectra recorded was essential to correct the background [20].

2.11. Fourier transform infrared (FTIR) spectroscopy

An overnight cell suspension of approximately 10^6 CFU mL^{-1} of *S. pyogenes* was prepared by including the MIC concentration of the compounds. Both the treated and control cells were harvested at 5000 g for 15 min. The pellets were washed thrice with MilliQ [43]. Twenty microliters of each bacterial sample was applied to the KBr disk and analyzed by FTIR (Bruker Optik GmbH, TENSOR 27) spectroscopy. Sixty-four scans were taken at a resolution of

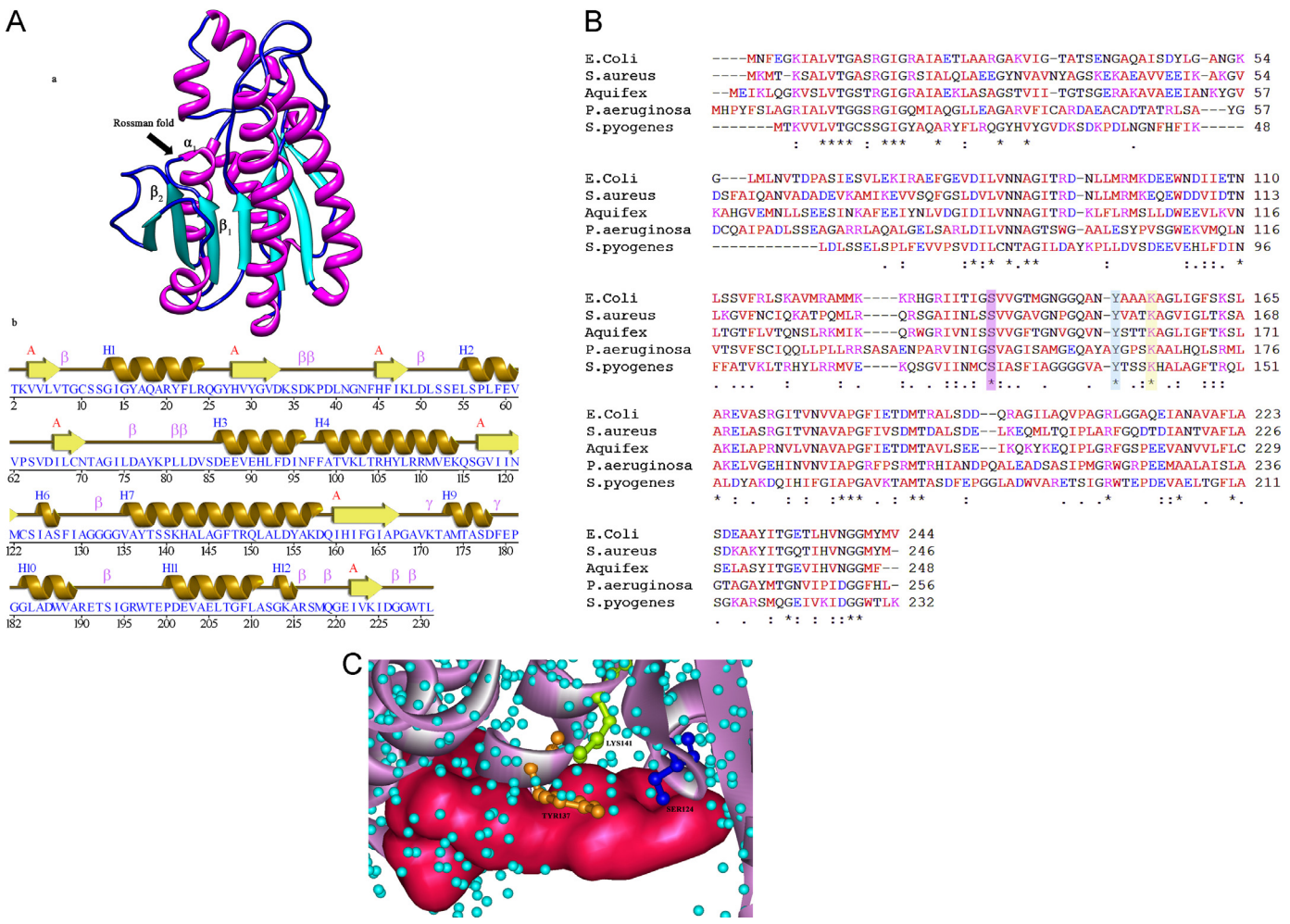

Fig. 1. (A) (a) Homology model of SPFabG generated using the template from PDB 2PNF. (b) Secondary structure prediction of the model using PROMOTIF analyses. (B) Multiple sequence alignment of FabG from different organisms with the highly conserved catalytic triad. (C) Binding site characterization of the protein SPFabG. The binding pocket is shown in pink, and the binding points in and around the pocket are shown as blue-colored balls.

4 cm^{-1}. All IR spectra were obtained in the range of 4000–400 cm^{-1} and were analyzed using the OPUS TM software.

2.12. Scanning electron microscopy (SEM)

The samples were prepared for SEM analysis as described by Di Pasqua [44]. After treatment with different compounds, the cells were harvested at 5000 g for 10 min and were washed twice with phosphate buffered saline (PBS). The control and treated cells were fixed in 2.5% glutaraldehyde for 1 h. Further, the samples were dehydrated through a graded series of ethanol (10–100%), allowed to dry for 10 min, gold sputtered and examined using a Hitachi S-3000H (Japan).

3. Results and discussion

3.1. Homology modeling

The secondary structure prediction of the modeled structure using PDBsum revealed the presence of one single short chain dehydrogenase (SDR) typical Rossman fold [45], which consisted of four β–α–β motifs covering the sequence from 2 to 225 aa (Fig. 1A). It is reported that the cofactor NADPH binds to this junction of two β–α–β–α–β motifs. SDR sequence motifs such as TGxxxGxG and NNAG, which are important for fold maintenance, are conserved [26]. Other important motifs are also conserved, such as the catalytic triad Ser124, Tyr137, Lys141 and the PG motif (181–182). In the absence of any crystal structure, homology modeling has been shown to be a valuable tool. For homology modeling of FabG, a BLAST search was performed, and the search results retrieved functionally and phylogenetically similar templates. Based on similarities, 2PNF (*A. aeolicus*), 3OSU (*S. aureus*), 3TZH (*Vibrio cholerae*), and 1I01 (*E. coli*) were in the order of 31% (1.8 Å), 26% (1.9 Å), 29% (2.10 Å) and 31% (2.6 Å) respectively. Due to its high resolution structure (1.8 Å) as well as comparatively better sequence identity (31%), the 2PNF protein was chosen as the template for the current study [26]. Using the MODELER module in DS Modeling 2.5, the skeletal backbone of the SPFabG was generated by copying the C_α coordinates of the aligned residues from the 2PNF.pdb file. The side chains with necessary insertions and deletions were modeled using automated or semi-automated procedures. Furthermore, the 3D model of SPFabG was refined using DS CHARMm, an energy minimization application, to relax unfavorable contacts [46]. The RMSD value of the target and the template was determined to be 1.65 Å, with the implication that the active site was preserved between the target and template so binding of the ligands was left largely unaffected (Supplementary Fig. 1A) [47].

Supplementary material related to this article can be found, in the online version, at http://dx.doi.org/10.1016/j.jmgm.2013.07.009.

Table 1
Ramachandran plot calculations on 3D model of SPFabG computed with the PROCHECK program.

SPFabG Residues involved in Ramachandran Plot	No of residues	% of residues
Residues in most favored regions	138	90.2
Residues in additional allowed regions	13	8.5
Residues in generously allowed regions	1	0.7
Residues in disallowed regions	1	0.7
Number of non-glycine and non-proline residues	153	100
Number of Glycine residues	16	
Number of proline residues	7	

The geometry of the final defined SPFabG model was evaluated using Ramachandran's plot calculation, computed with the PROCHECK program (Table 1). The Phi/Psi distribution shows that 90.2% of the residues in the SPFabG model are in the most favored or allowed regions (Supplementary Fig. 1B). The Ser64 and Ala130 amino acids present in the disallowed regions of the Ramachandran plot are not conserved between the target and template and thus do not impart any significant change in the final conformation of the modeled structure (SPFabG). The superimposition of the SPFabG model with the template showed RMSD of 1.65 Å. Furthermore, these two residues (Ser64 and Ala130) that are present in the short loops play a significant role in connecting two secondary structural elements of SPFabG. The Ala130 predicted to be present in the binding region does not show any interactions with the small molecules. Hence, these two residues are determined to be functionless, except for their involvement in the connection of the structural elements in the protein [48]. The ERRAT factor, a second calculation used to validate the overall quality of SPFabG, is 76.923 (Supplementary Fig. 1C) and the G-factor was computed to be 0.04. Thus, the SPFabG homology model, which satisfies all of the validation criteria, was used for further studies.

Supplementary material related to this article can be found, in the online version, at http://dx.doi.org/10.1016/j.jmgm.2013.07.009.

3.2. Binding site prediction

The binding pocket identification in SPFabG revealed the presence of the active site residues Ala77, Ser124, Gly133, Tyr137, Lys141, Ala169 and Asp178, which are involved in the binding of the natural cofactor NADPH (Supplementary Fig. 1D). Among these residues, the catalytic residues (Ser124, Tyr137 and Lys141) were found to be highly conserved among SDRs of other organisms (Figs. 1B and C). This finding indicates that the cofactor-binding mode should be very similar among type I and type II fatty acids [49]. According to Oppermann et al. (in 2003), a short chain dehydrogenase region (SDR) encloses the active residues (Ser, Tyr and Lys) that are essential for cofactor (NADPH) binding. The SDR

Table 2
The top thirteen ligands of high docking score and their interactions with catalytic residues.

Compound name	PubChem ID	Docking score	Binding energy (kcal mol^{-1})	Atomic interactions		
				Donor	Acceptor	Distance in Å
EGC	72277	54. 464	752.54	Lig(H34)	SER124(O)	2.21
				Lig(H36)	TYR137(O)	2.27
				LYS141(H23)	Lig(O)	1.903
				Lig(H32)	ASN70(O)	1.62
GCG	199472	45.31	394.15	SER124(HG)	Lig(O6)	2.31
				Lig(H48)	SER124(O4)	1.83
				GLY134	Lig(O9)	2.09
				Lig(H51)	GLY133(O)	2.44
ECG	65056	44.42	−88.01	Lig(H42)	ASP178(OD2)	2.36
				Lig(H47)	TYR137(OH)	2.34
EC	72276	42.31	390.36	TYR137(HH)	Lig(O4)	1.52
				Lig(H33)	TYR137(OH)	2.46
EGCG	65064	39.938	945.18	Lig(H43)	TYR137(OH)	1.36
				VAL170(HN)	Lig(H43)	2.17
				Lig(H51)	ASP178(OD1)	2.42
Catechin	6419835	37.925	10.14	Lig(H43)	SER124(OG)	1.83
				TYR137(HH)	Lig(O4)	2.29
				HIS142(HN)	Lig(O3)	2.20
Propyl Gallate	4947	33.491	696.784	Lig(H25)	AP76((OD1)	2.0
				Lig(H27)	GLU88(OE2)	1.53
Rosmaric acid	5281792	33.32	529.02	Lig(H40)	Ala77(O)	1.11
				Ala77(HN)	Lig(O3)	2.20
				TYR137(HH)	Lig(O8)	2.40
				Lig(H41)	TYR137(OH)	2.49
Curcumin	969516	30.936	−16.12	Lig (H41)	ASP178(OD2)	1.467
Cerulenin	5352018	30.087	480.25	Lig(H25)	LYS141(O)	2.43
				Lig(H24)	LYS141(O)	1.41
				SER124(HN)	Lig(O2)	1.04
				SER124(HG)	Lig(O1)	1.04
Luteolin[a]	5280445	30.08	658.43	Lig(H29)	GLU88(OE1)	1.41
Eugenol[a]	3314	26.371	−39.45	SER124(HG)	Lig(O2)	2.33
Safrole	5144	13.994	−16.02	SER124(HG)	Lig(O1)	2.09

[a]Sigma-pi interaction- Luteolin-ASP83; Eugenol-LYS224

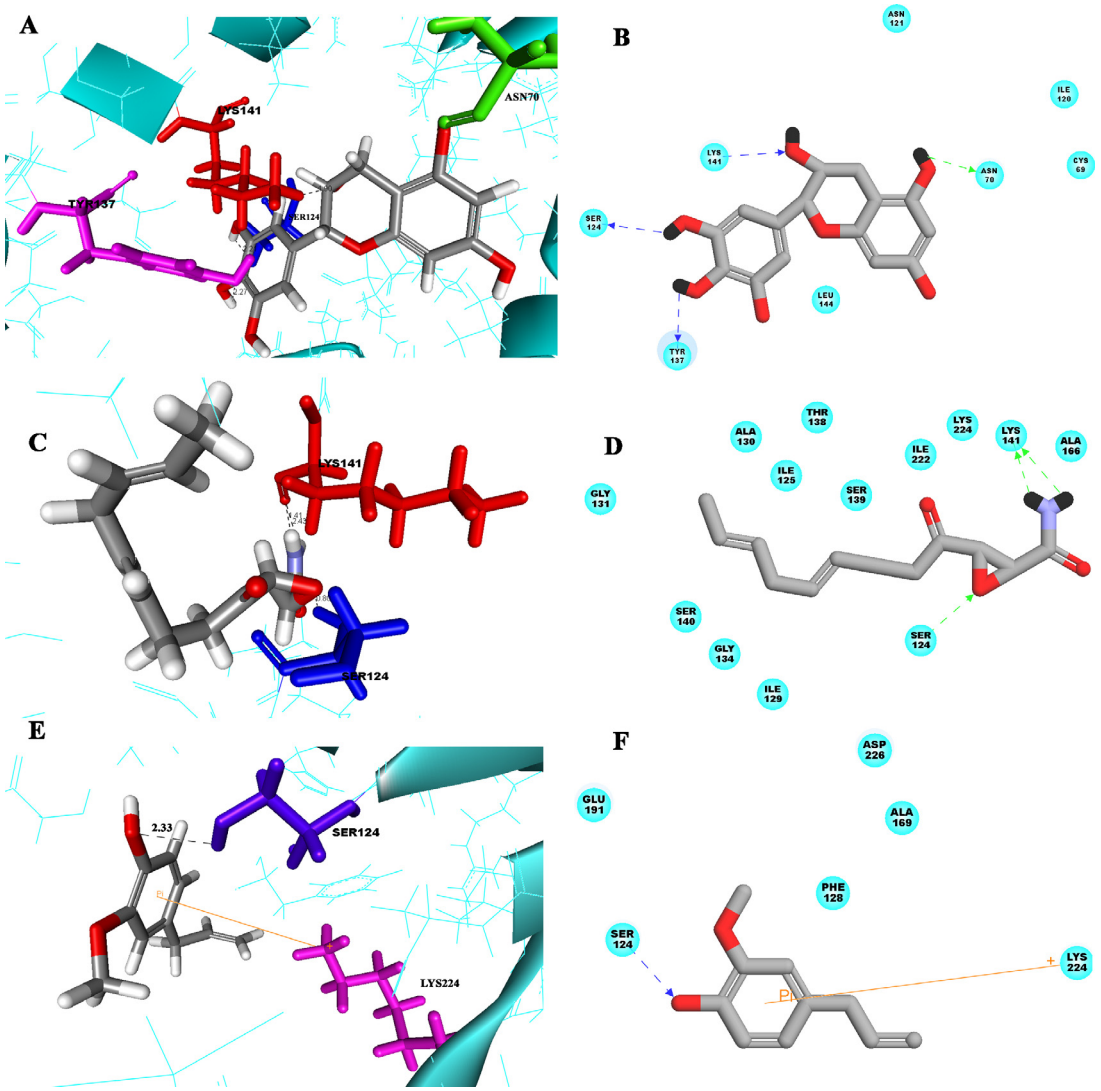

Fig. 2. Docking orientation of the ligands in the active binding site of SPFabG, represented in 3D and 2D; (A) EGC binding to the catalytic triad (SER124, TYR137 and LYS141), (B) representation of the 2D interaction of EGC with active residues; (C) Cerulenin binding to SER124 and LYS141, (D) 2D interaction of CER with active residues; (E) Eugenol binding to SER124 and showing pi interaction with LYS224, and (F) 2D interaction of EUG with the active residues.

family members, with their known structure, rearrange their active site residues upon cofactor binding. Sequence alignment (Fig. 1B) and superimposition (Supplementary Fig. 1A) of SPFabG with other SDRs indicate the presence of these highly conserved active residues in the SDR of SPFabG. Thus, the constructed homology model is expected to bind with NADPH, similar to other SDRs, and may be involved in the catalysis process. Thus, the presence of the domain (SDR) could assist the protein in NADPH-dependent biological processes. The region where the natural ligand interacts is defined to be the binding pocket of SPFabG, so the test ligands were docked into this region.

Supplementary material related to this article can be found, in the online version, at http://dx.doi.org/10.1016/j.jmgm.2013.07.009.

3.3. Docking of inhibitors

Molecular docking was performed against the ligand database generated from PubChem. Among the 60,485 ligands in the database, 2500 candidates were able to successfully interact with the receptor; among these 2500, the top 13 compounds with the highest score are shown in Table 2. Five amino acids present in the binding site provided the necessary hydrophobic environment. Among the 13 ligands, the highest scoring compound, EGC, with a dock score of 54.464, showed strong interactions with catalytic triad present in the binding pocket (Fig. 2A andB). Thus, most of the 13 ligands are donors that share a hydrogen bond with the acceptor atom (either nitrogen or oxygen) and bring about a strong interaction with the active residues (Supplementary Fig. 2A–J). For an effective docking study, hydrogen bonding interaction depends on the donor and the acceptors present in the protein and ligands. A donor atom that has the capacity to donate its hydrogen atom to form bonding bridges in the acceptor region is referred to as the hydrogen bond donor (HBD), and the atoms that have the capacity to accept the donated hydrogen atoms are called hydrogen bond acceptors (HBAs). EGC, a component of green tea, forms strong hydrogen bonds by accepting oxygen atoms from SER124 (2.21 Å), TYR137 (2.27 Å) and ASN70 (1.62 Å) and donates a hydrogen atom of TYR137 (1.90 Å) to an oxygen atom of the EGC with the highest binding energy of 752.54 kcal mol^{-1}. CER, which has been well characterized as a potent FAS II inhibitor [50], donates the hydrogen atoms (H25 and H24) to an oxygen atom of LYS141 (2.43 Å; 1.41 Å), thus forming two hydrogen bonds with binding energy of 480.25 kcal mol^{-1} (Fig. 2C and D). EUG, a compound found in clove

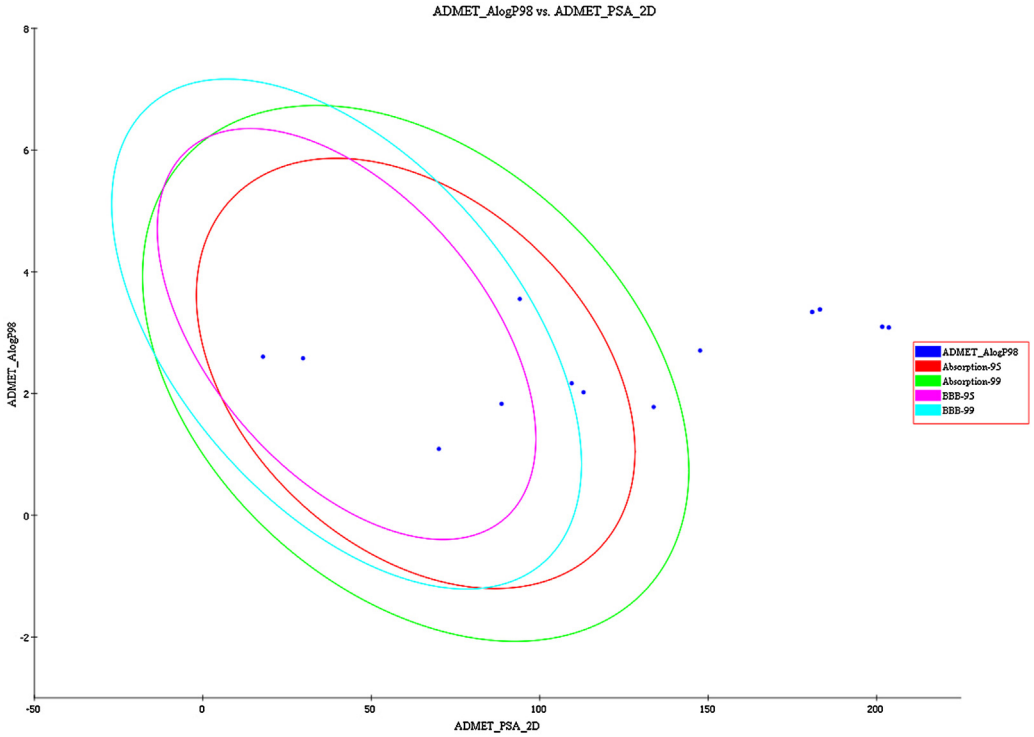

Fig. 3. ADMET plot of polar surface area *versus* AlogP for the 13 descriptors.

oil, shares an oxygen atom with a hydrogen atom of SER124 (2.33 Å) (Figs. 2E–F), with the least binding energy of -39.45 kcal mol^{-1}. The dock complexes of CER were used as the positive control and the dock complexes of the ligands with highest (EGC) and lowest (EUG) binding energy were further selected for MD simulation. The hydrogen bonding formed between the HBD and HBA of the other ligands with the receptor are presented in Table 2.

Supplementary material related to this article can be found, in the online version, at http://dx.doi.org/10.1016/j.jmgm.2013.07.009.

3.4. ADMET prediction

The ADMET descriptor represents the models that produce the characteristics of ADMET properties. The plot of polar surface area (PSA) *versus* A log P is shown in Fig. 3. The ligands GCG, Catechin, ECG, Rosmaric acid, and Cerulenin are located outside the accepted region of ADMET in the plot, which indicates that other compounds have good ADMET properties. Thus EGC and EUG, which are present in the acceptable regions, and CER, which is outside the accepted ADMET plot region, were further selected for MD simulation for a comparative assessment.

3.5. Molecular dynamics simulation

To validate the docking results, the dynamical behaviors of the receptor and the ligand complexes were explored. An MD simulation run of approximately 10 ns was evaluated for both the apo and holo forms. During the simulation, the root mean square deviation (RMSD) values increased very rapidly during the first 0.8 ns. This increase generally occurs because the structures relax, when being dissolved in the solution. Fig. 4A presents the backbone RMSD plot of the apo and holo forms. The RMSD of the apo form was 0.38 Å at the time point of 3.0 ns. The RMSD of NADPH complex was 0.1 Å and remained to be stable throughout MD simulation. The ligand complexes of EGC, CER and EUG at 3.0 ns were 0.35 Å, 0.43 Å and 0.30 Å, respectively. The holo forms showed a noticeable deviation between 2.0 and 3.0 ns, after which the complexes remained stable until the end. The overall dynamic stability of EGC and CER showed only a slight deviation. In contrast, the EUG complex showed a wide range of variation in overall conformation. This result is likely due to EUG's sigma-pi interaction with Lys224, which might have distorted its structure and thereby prevented its contact with other residues. Conversely, examining the fluctuations in the Cα atom revealed that the apo form shows fluctuation compared to the docked complexes, which remain stable after binding the ligands. The main characteristics of the SDR family enzymes are upon substrate binding the protein undergoes conformational changes. The substrate binding loop of the apoenzyme will have open conformation. Binding of NADPH to the loop showed closed conformation [51]. Thus from the overall data of MD simulation an average RMSD of approximately 0.73, 0.8, 0.7 and 0.9 Å was observed for apo form and holo forms of EGC, CER and EUG respectively. The NADPH complex showed an average RMSD of approximately 0.2 Å. The RMSD values of the final conformers showed only a slight deviation from their initial conformer and remained to be stable during the MD simulation. The potential energy (PE) is a simple measure to check the stability of the system. The PE plot as a function of time showed that during the course of simulation PE was minimum for all the inhibitor-protein complexes (EGC, CER and EUG) compared to NADPH-protein complex (Fig. 4C). Also the RMSF plot was calculated to study the flexibility of the aminoacids in the complex. Although slight differences were observed in the apo and holo forms, their overall patterns in the RMSF trajectories are quite similar (Fig. 4B). The binding free energy (ΔG_{bind}) calculation (Table 3) for receptor–ligand complexes after MD simulation showed the free energy of −37.35 kcal mol^{-1} for NADPH, −38.52 kcal mol^{-1} for EGC, −35.06 kcal mol^{-1} for CER and −29.26 kcal mol^{-1} for EUG. The binding energy of EGC was high compared to the cofactor (NADPH) and other test compounds (CER and EUG) after MD simulation.

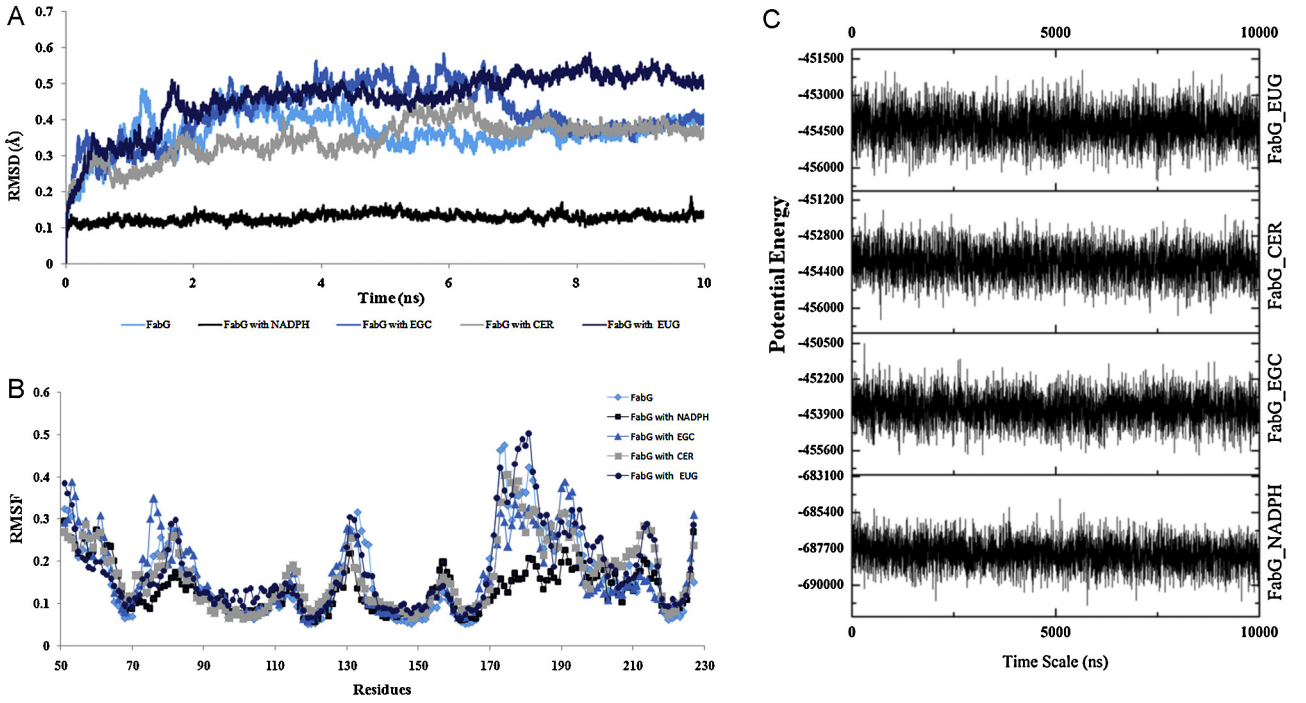

Fig. 4. (A) Comparison of RMSD backbone of the apo and holo forms from the trajectory of 10 ns MD simulation. (B) RMSF of the apo and holo forms in the dynamic state. The plot represents the RMSF over 10 ns. (C) Potential energy plot for apo and holo forms representing the stability of the system.

3.6. Antimicrobial activity test

The ligands (EGC, CER and EUG) were further screened for antibacterial activity. CER inhibits bacterial growth at differing concentrations depending on the species and the growth conditions [52]. In the present study, the antibacterial activity of CER was observed at 20 and 200 μM concentrations, and the zones of inhibition were found to be 13 and 20 mm, respectively. The antibacterial activity of EGC and EUG was investigated between 0.2 and 2800 μM. The zone of inhibition was found to be 12 mm at 200 μM for EGC. EUG failed to show any zone of clearance, even at 2800 μM. The MIC values of CER and EGC were observed to be 20 μM mL^{-1} and 200 μM mL^{-1}, respectively. This result clearly shows that CER and EGC act as promising antibacterial agents compared to a negative control (Eugenol).

3.7. Inhibition of FabG

The results of the docking studies showed that CER and EGC have the potential to bind directly to the free enzyme. Further spectrophotometric analysis substantiated the results of the docking studies. Fig. 5 illustrates that CER and EGC exhibit significant ($P < 0.05$) inhibitory activity against the enzyme in a concentration-dependent manner compared to EUG. The IC_{50} was recorded as 2.9 ± 1.51 μg/ml for CER and 14.57 ± 0.50 μg/ml for EGC. The inhibitors CER and EGC exhibited the highest inhibitory activity of 67.53 and 53.24% compared with EUG. According to an earlier study [53], FabG undergoes a series of complex conformational changes in response to NADPH binding to the active site region of the protein. The results of the *in vitro* analysis corroborate the *in silico* analysis nicely, wherein CER and EGC are able to inhibit the enzyme (FabG) and prevent the conversion of the substrate into the respective end product.

Table 3
The MM-GBSA binding free energies (kcal mol^{-1}) of FabG and their ligands (NADPH, EGC, CER and EUG) before and after molecular dynamics simulations.

FabG interaction	ΔG_{bind} (kcal mol^{-1})	
	Before simulation	After simulation
NADPH	−38.74	−37.35
EGC	−33.93	−38.52
CER	−35.30	−35.06
EUG	−32.34	−29.26

3.8. Fluorescence analysis

The effect of ligands on binding to FabG in *S. pyogenes* was investigated using spectrofluorimetry. The excitation and emission spectra recorded on binding of the ligands to FabG are shown in Fig. 6a and b. Upon the binding of NADPH to FabG, the enzyme converts the substrate acetoacetyl-CoA into (*R*)-3-HB-CoA [54]. An increase in fluorescence intensity was observed with the increase in the conversion of the substrate. The binding of the ligand to the enzyme prevents the conversion of the

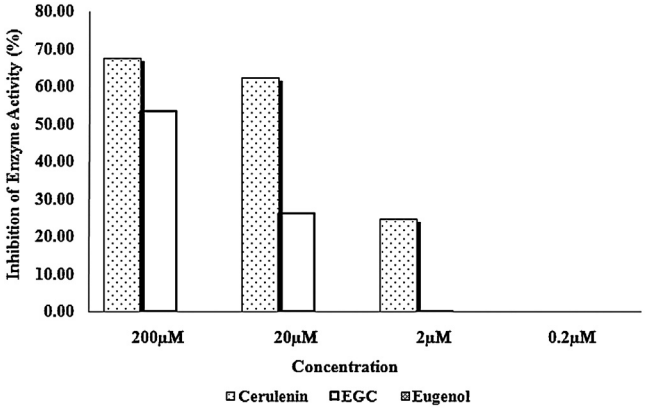

Fig. 5. Inhibition of FabG activity by different concentrations of the inhibitors (CER, EGC and EUG).

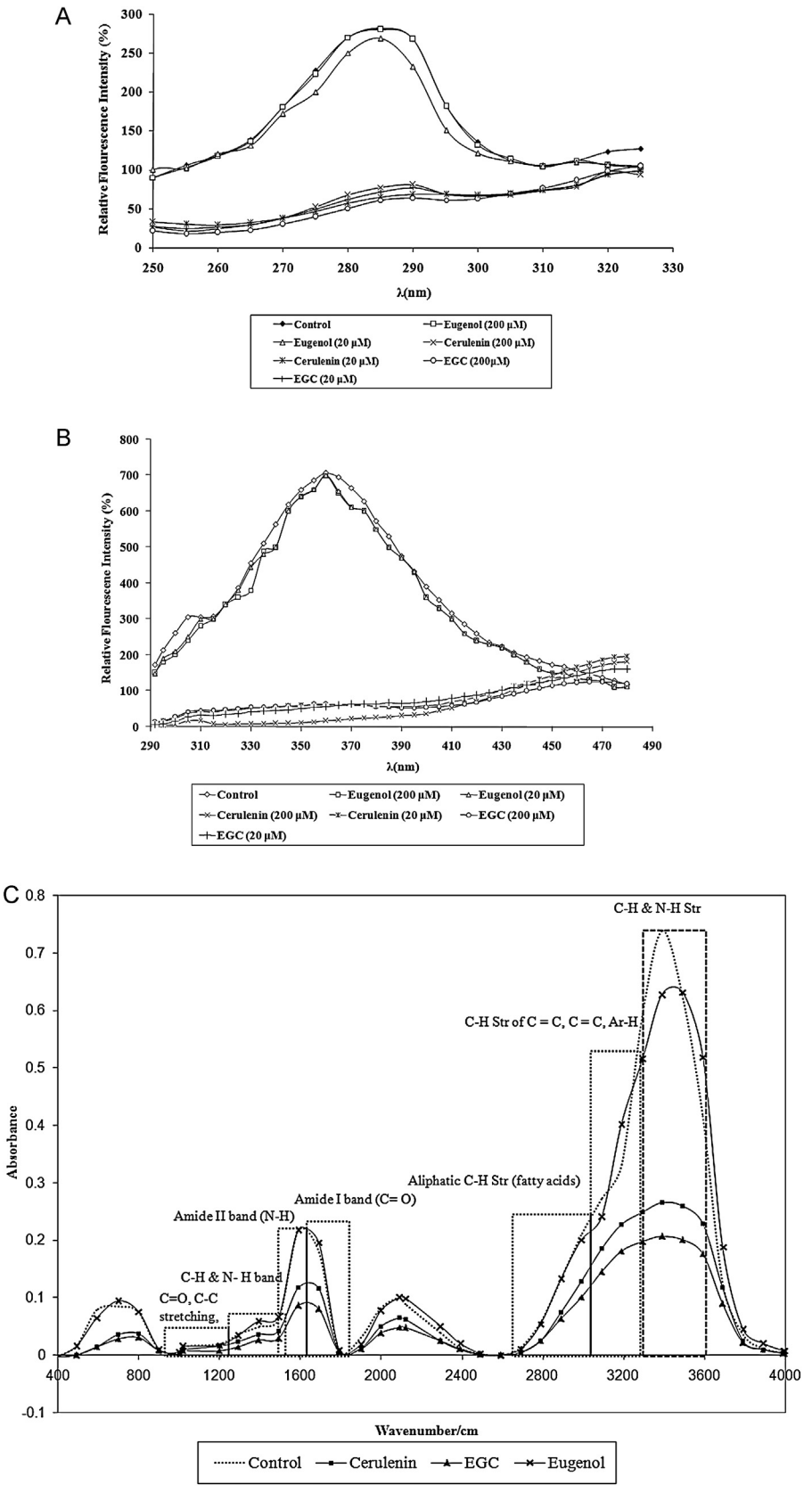

Fig. 6. Inhibitory effects of conformers on FabG. (a) Fluorescence emission spectra; (b) fluorescence excitation spectra; (c) comparison of the FTIR spectra of the *S. pyogenes* control and treated (CER, EGC and EUG), represented in the mid-infrared region (400–4000 cm^{-1}). Characteristic functional groups contributing to the formation of absorption bands at specific wavenumbers are indicated in the figure.

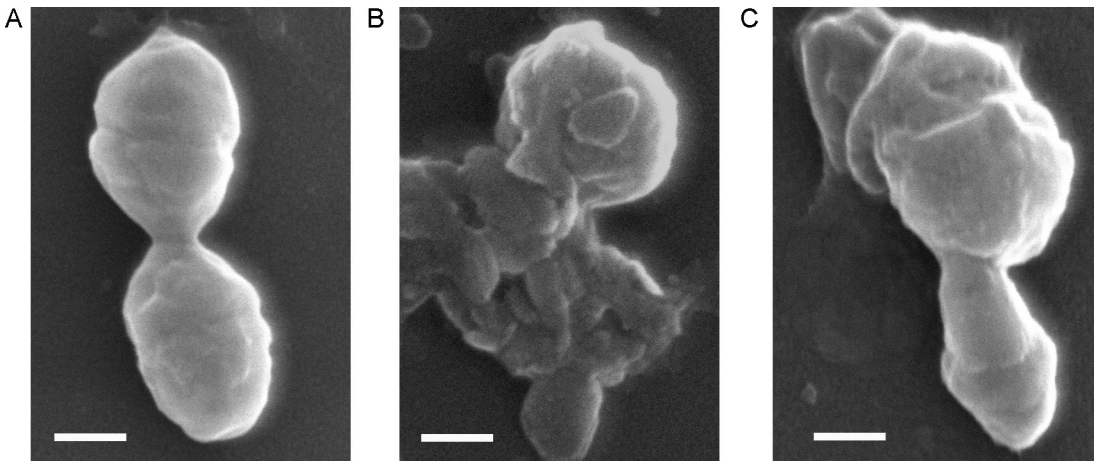

Fig. 7. Scanning electron micrographs of cells of untreated and treated *S. pyogenes*. (a) Control; (b) CER (20 μM mL^{-1}); (c) EGC (200 μM mL^{-1}) (scale bar = 1 μm).

substrate, which is recorded as a decrease in fluorescence intensity. Thus, the excitation and emission plot confirm that CER and EGC inhibit FabG, compared to EUG. In addition, a competitive inhibition occurred between the cofactor NADPH and the ligands. CER and EGC were assumed to have sterical conflict with NADPH, thus allowing them to oxidize ($NADP^+$), and the oxidized form was unable to bind the enzyme (FabG) [55]. The interaction studies with fluorescence spectroscopy thus corroborate the docking studies and reveal EGC as a potent inhibitor compared to EUG.

3.9. Infrared spectroscopy

Fatty acids are the building blocks essential for cell membrane formation and the production of virulence factors in *S. pyogenes*. The effect of these ligands (CER, EGC and EUG) on the total lipid content of *S. pyogenes* was analyzed using FTIR. The lipid content extracted from the control and the treated cells of *S. pyogenes* revealed major changes in the assignment of H-bonded OH groups and NH_2 stretching (3280 cm^{-1}). An important frequency displacement of aliphatic C—H stretching (fatty acids) at a frequency between 2960–2920 cm^{-1} and 1300–1390 cm^{-1} in the region corresponding to membrane fatty acids is shown in Fig. 6c. Thus, it is presumed that the chemical shift in the control and treated spectra of *S. pyogenes* substantiates the fact that the ligands have inhibited the intermediate fatty acid pathway protein (FabG), which, in turn, prevents the synthesis and completion of the fatty acid pathway and shuts down the other lipid-mediated cellular mechanisms of the pathogen.

3.10. SEM

Changes in the appearance of cells of *S. pyogenes* before and after the treatment with the natural antimicrobial compounds are illustrated in Fig. 7a–c. In control groups, the untreated cells had smooth walls. In contrast, obvious detrimental effects on the morphology of the cell membrane of *S. pyogenes* were observed when treated with the MIC values of the compounds. CER (20 μM) and EGC (200 μM) were able to alter the structure of the outer envelope and disrupt the membrane, thus allowing the leakage of intracellular constituents [56,57]. This result suggests a mechanism of action of these compounds against the outer cell envelope, most likely interacting with the membrane lipid profile and causing membrane structural alterations appreciable by SEM examination. These results again confirm that bacterial fatty acid synthesis can be used as an optimal target of many antibacterial agents [58]. Thus, FabG, an enzyme involved in the lipids biosynthesis pathway of *S. pyogenes*, appears to be an important target for the development of novel antimicrobials.

4. Conclusion

S. pyogenes causes contagious diseases such as strep throat infections that are transmitted from one person to another. It has already been reported that FabG is an essential enzyme involved in the elongation cycle of the fatty acid biosynthesis pathway. In general, fatty acids are essential for cell wall formation and the intermediates synthesized during the biosynthesis have essential roles in quorum sensing and virulence factor production. Thus, in the present study, a structure-based drug design approach was developed and applied to identify inhibitors of FabG in *S. pyogenes*. Currently, a co-crystal structure for FabG from *S. pyogenes* with the inhibitor or the substrate to the binding site is unavailable. Therefore, a homology model of FabG from *S. pyogenes* was generated, employing a multiple template spatial restraints method for structure-based design. A large dataset of compounds was screened against SPFabG. Furthermore, MD was performed to check the stability of the ligands (EGC, CER and EUG) in their complexes. The MD results revealed that EGC and CER are highly stable without altering their interactions. *In vitro* biological assays were performed and confirmed that the compounds EGC and CER significantly inhibit the fatty acid profile of the pathogen. From the experimental analysis, we obtained significant results delineating the FabG inhibitory activity by EGC compared with the well-studied control ligand CER. Its possible mode of action was also elucidated. Because EGC is a natural (herbal) ligand, it is expected to provide a modest mode of inhibition and a few added benefits, such as ease in oral intake and reduced immunogenicity. Thus, from the results of the present study, it is strongly suggested that EGC is a potent inhibitor of FabG that should be further explored as a potential drug candidate for *S. pyogenes*-related infections.

Acknowledgements

The authors gratefully acknowledge the computational and bioinformatics facility provided by the Alagappa University Bioinformatics Infrastructure Facility (funded by DBT, GOI; Grant No. BT/BI/25/001/2006). The financial support provided in the form of SRF to RMBS by CSIR, HRDG (9/688(0012)/2011) is gratefully acknowledged. The authors thankfully acknowledge Chandrabose

Selvaraj and Dr. Sanjeev Kumar Singh from Computer Aided Drug Design and Molecular Modelling Lab, Department of Bioinformatics, Alagappa University for helping us in using Schrodinger V9.2 LLC, New York, NY 2011, for our studies.

References

[1] M.W. Cunningham, Pathogenesis of group A streptococcal infections, Clinical Microbiology Reviews 13 (2000) 470–511.
[2] S. Malhotra-Kumar, C. Lammens, J. Piessens, H. Goossens, Multiplex PCR for simultaneous detection of macrolide and tetracycline resistance determinants in streptococci, Antimicrobial Agents and Chemotherapy 49 (2005) 4798–4800.
[3] A.G. Michos, C.G. Bakoula, M. Braoudaki, F.I. Koutouzi, E.S. Roma, A. Pangalis, G. Nikolopoulou, E. Kirikou, V.P. Syriopoulou, Macrolide resistance in *Streptococcus pyogenes*: prevalence, resistance determinants, and emm types, Diagnostic Microbiology and Infectious Disease 64 (2009) 295–299.
[4] I. Karaman, F. Sahin, M. Gulluce, H. Ogutcu, M. Sengul, A. Adiguzel, Antimicrobial activity of aqueous and methanol extracts of *Juniperus oxycedrus* L., Journal of Ethnopharmacology 85 (2003) 231–235.
[5] A. Sanchez-Medina, K. Garcia-Sosa, F. May-Pat, L.M. Pena-Rodriguez, Evaluation of biological activity of crude extracts from plants used in Yucatecan traditional medicine part I. Antioxidant, antimicrobial and beta-glucosidase inhibition activities, Phytomedicine 8 (2001) 144–151.
[6] K.R. Cheruiyot, D. Olila, J. Kateregga, In-vitro antibacterial activity of selected medicinal plants from Longisa region of Bomet district, Kenya, African Health Sciences 9 (Suppl. (1)) (2009) S42–S46.
[7] S. Hemaiswaryaa, A.K. Kruthiventib, M. Doble, Synergism between natural products and antibiotics against infectious diseases, Phytomedicine 15 (2008) 639–652.
[8] T. Puig, J. Relat, P.F. Marrero, D. Haro, J. Brunet, R. Colomer, Green tea catechin inhibits fatty acid synthase without stimulating carnitine palmitoyltransferase-1 or inducing weight loss in experimental animals, Anticancer Research 28 (2008) 3671–3676.
[9] A.B. Sharangi, Medicinal and therapeutic potentialities of tea (Camellia sinensis L.) – a review, Food Research International 42 (2009) 529–535.
[10] J.M. Song, B.L. Seong, Tea catechins as a potential alternative anti-infectious agent, Expert Review of Anti-infective Therapy 5 (2007) 497–506.
[11] R.J. Heath, C.O. Rock, Fatty acid biosynthesis as a target for novel antibacterials, Current Opinion in Investigational Drugs 5 (2004) 146–153.
[12] M.J. Sohn, C.J. Zheng, W.G. Kim, S. Macrolactin, a new antibacterial agent with FabG-inhibitory activity from Bacillus sp. AT28, Journal of Antibiotics 61 (2008) 687–691.
[13] S. Brinster, G. Lamberet, B. Staels, P. Trieu-Cuot, A. Gruss, C. Poyart, Type II fatty acid synthesis is not a suitable antibiotic target for gram-positive pathogens, Nature 458 (2009) 83–86.
[14] Y. Shen, J. Liu, G. Estiu, B. Isin, Y.Y. Ahn, D.S. Lee, A.L. Barabasi, V. Kapatral, O. Wiest, Z.N. Oltvai, Blueprint for antimicrobial hit discovery targeting metabolic networks, Proceedings of the National Academy of Sciences of the United States of America 107 (2010) 1082–1087.
[15] J.B. Parsons, C.O. Rock, Is bacterial fatty acid synthesis a valid target for antibacterial drug discovery? Current Opinion in Microbiology 14 (2011) 544–549.
[16] Y.J. Kwon, M.J. Sohn, T. Oh, S.N. Cho, C.J. Kim, W.G. Kim, Panosialins, inhibitors of enoyl-ACP reductase from *Streptomyces* sp. AN1761, Journal of Microbiology and Biotechnology 23 (2013) 184–188.
[17] Q. Zhang, C. Yu, J. Min, Y. Wang, J. He, Z. Yu, Rational questing for potential novel inhibitors of FabK from *Streptococcus pneumoniae* by combining FMO calculation, CoMFA 3D-QSAR modeling and virtual screening, Journal of Molecular Modeling 17 (2011) 1483–1492.
[18] R. Thenmozhi, K. Balaji, M. Kanagavel, S.K. Karutha, Development of species-specific primers for detection of *Streptococcus pyogenes* from throat swabs, FEMS Microbiology Letters 306 (2010) 110–116.
[19] T.T. Hoang, S.A. Sullivan, J.K. Cusick, H.P. Schweizer, Beta-ketoacyl acyl carrier protein reductase (FabG) activity of the fatty acid biosynthetic pathway is a determining factor of 3-oxo-homoserine lactone acyl chain lengths, Microbiology 148 (2002) 3849–3856.
[20] S. Ducasse-Cabanot, M. Cohen-Gonsaud, H. Marrakchi, M. Nguyen, D. Zerbib, J. Bernadou, M. Daffe, G. Labesse, A. Quemard, In vitro inhibition of the Mycobacterium tuberculosis beta-ketoacyl-acyl carrier protein reductase MabA by isoniazid, Antimicrobial Agents and Chemotherapy 48 (2004) 242–249.
[21] D. Tasdemir, G. Lack, R. Brun, P. Ruedi, L. Scapozza, R. Perozzo, Inhibition of *Plasmodium falciparum* fatty acid biosynthesis: evaluation of FabG, FabZ, and FabI as drug targets for flavonoids, Journal of Medicinal Chemistry 49 (2006) 3345–3353.
[22] J.Y. Lee, K.W. Jeong, S. Shin, J.U. Lee, Y. Kim, Antimicrobial natural products as beta-ketoacyl-acyl carrier protein synthase III inhibitors, Bioorganic and Medicinal Chemistry 17 (2009) 5408–5413.
[23] Y.M. Zhang, C.O. Rock, Evaluation of epigallocatechin gallate and related plant polyphenols as inhibitors of the FabG and FabI reductases of bacterial type II fatty-acid synthase, Journal of Biological Chemistry 279 (2004) 30994–31001.
[24] S.F. Altschul, W. Gish, W. Miller, E.W. Myers, D.J. Lipman, Basic local alignment search tool, Journal of Molecular Biology 215 (1990) 403–410.
[25] H.M. Berman, T.N. Bhat, P.E. Bourne, Z. Feng, G. Gilliland, H. Weissig, J. Westbrook, The Protein Data Bank and the challenge of structural genomics, Natural Structural Biology 7 (Suppl) (2000) 957–959.
[26] Q. Mao, W.L. Duax, T.C. Umland, Crystallization, X-ray diffraction analysis of the beta-ketoacyl-acyl carrier protein reductase FabG from *Aquifex aeolicus* VF5, Acta Crystallographica Section F: Structural Biology and Crystallization Communications 63 (2007) 106–109.
[27] A. Sali, T.L. Blundell, Comparative protein modelling by satisfaction of spatial restraints, Journal of Molecular Biology 234 (1993) 779–815.
[28] S. Fan, Q. Geng, Z. Pan, X. Li, L. Tie, Y. Pan, Clarifying off-target effects for torcetrapib using network pharmacology and reverse docking approach, BMC Systems Biology 6 (2012) 152.
[29] D.J. Miller, Y.M. Zhang, C.O. Rock, S.W. White, Structure of RhlG, an essential beta-ketoacyl reductase in the rhamnolipid biosynthetic pathway of *Pseudomonas aeruginosa*, Journal of Biological Chemistry 281 (2006) 18025–18032.
[30] C.M. Venkatachalam, X. Jiang, T. Oldfield, M. Waldman, LigandFit: a novel method for the shape-directed rapid docking of ligands to protein active sites, Journal of Molecular Graphics and Modelling 21 (2003) 289–307.
[31] Y. Zhao, J. Wang, Y. Wang, J. Huang, A comparative analysis of protein targets of withdrawn cardiovascular drugs in human and mouse, Journal of Clinical Bioinformatics 2 (2012) 10.
[32] P. Ponnan, S. Gupta, M. Chopra, R. Tandon, S.A. Baghel, G. Gupta, A.K. Prasad, R.C. Rastogi, M. Bose, H.G. Raj, 2D-QSAR, docking studies, and in silico ADMET prediction of polyphenolic acetates as substrates for protein acetyltransferase function of glutamine synthetase of mycobacterium tuberculosis, ISRN Structural Biology 2013 (2012) 1–12.
[33] A.W. Schuttelkopf, D.M. van Aalten, PRODRG: a tool for high-throughput crystallography of protein–ligand complexes, Acta Crystallographica Section D: Biological Crystallography 60 (2004) 1355–1363.
[34] M. Baran, J. Mazerski, Molecular modelling of membrane sterols with the use of the GROMOS 96 force field, Chemistry and Physics of Lipids 120 (2002) 21–31.
[35] R.M. Shafreen, C. Selvaraj, S.K. Singh, S.K. Pandian, Exploration of fluoroquinolone resistance in *Streptococcus pyogenes*: comparative structure analysis of wild-type and mutant DNA gyrase, Journal of Molecular Recognition 26 (2013) 276–285.
[36] S.K. Tripathi, S.K. Singh, P. Singh, P. Chellaperumal, K.K. Reddy, C. Selvaraj, Exploring the selectivity of a ligand complex with CDK2/CDK1: a molecular dynamics simulation approach, Journal of Molecular Recognition 25 (2012) 504–512.
[37] R. Thenmozhi, P. Nithyanand, J. Rathna, S.K. Pandian, Antibiofilm activity of coral-associated bacteria against different clinical M serotypes of *Streptococcus pyogenes*, FEMS Immunology and Medical Microbiology 57 (2009) 284–294.
[38] R.J. Heath, C.O. Rock, Enoyl-acyl carrier protein reductase (fabI) plays a determinant role in completing cycles of fatty acid elongation in *Escherichia coli*, Journal of Biological Chemistry 270 (1995) 26538–26542.
[39] C.Y. Lai, J.E. Cronan, Isolation and characterization of beta-ketoacyl-acyl carrier protein reductase (fabG) mutants of *Escherichia coli* and *Salmonella enterica* serovar Typhimurium, Journal of Bacteriology 186 (2004) 1869–1878.
[40] M.M. Bradford, A rapid and sensitive method for the quantitation of microgram quantities of protein utilizing the principle of protein–dye binding, Analytical Biochemistry 72 (1976) 248–254.
[41] R.E. Toomey, S.J. Wakil, Studies on the mechanism of fatty acid synthesis. XVI. Preparation and general properties of acyl-malonyl acyl carrier protein-condensing enzyme from *Escherichia coli*, Journal of Biological Chemistry 241 (1966) 1159–1165.
[42] N. Suganthy, P. Kesika, S. Karutha, P. Kasi, P. Devi, Mangrove plant extracts: radical scavenging activity and the battle against food-borne pathogens, Forschende Komplementarmedizin 16 (2009) 41–48.
[43] D. Bizani, A.S. Motta, J.A. Morrissy, R.M. Terra, A.A. Souto, A. Brandelli, Antibacterial activity of cerein 8A, a bacteriocin-like peptide produced by *Bacillus cereus*, International Microbiology 8 (2005) 125–131.
[44] R. Di Pasqua, G. Betts, N. Hoskins, M. Edwards, D. Ercolini, G. Mauriello, Membrane toxicity of antimicrobial compounds from essential oils, Journal of Agricultural and Food Chemistry 55 (2007) 4863–4870.
[45] M.G. Rossmann, P. Argos, Protein folding, Annual Review of Biochemistry 50 (1981) 497–532.
[46] A. Nayeem, D. Sitkoff, S. Krystek Jr., A comparative study of available software for high-accuracy homology modeling: from sequence alignments to structural models, Protein Science 15 (2006) 808–824.
[47] N.L. Summers, M. Karplus, Construction of side-chains in homology modelling. Application to the C-terminal lobe of rhizopuspepsin, Journal of Molecular Biology 210 (1989) 785–811.
[48] D. Pal, P. Chakrabarti, On residues in the disallowed region of the Ramachandran map, Biopolymers 63 (2002) 195–206.
[49] U. Oppermann, C. Filling, M. Hult, N. Shafqat, X. Wu, M. Lindh, J. Shafqat, E. Nordling, Y. Kallberg, B. Persson, H. Jornvall, Short-chain dehydrogenases/reductases (SDR): the 2002 update, Chemico-Biological Interactions 143-144 (2003) 247–253.
[50] L.Y. Gao, F. Laval, E.H. Lawson, R.K. Groger, A. Woodruff, J.H. Morisaki, J.S. Cox, M. Daffe, E.J. Brown, Requirement for kasB in Mycobacterium mycolic acid biosynthesis, cell wall impermeability and intracellular survival: implications for therapy, Molecular Microbiology 49 (2003) 1547–1563.
[51] A.T. Marques, P.A. Fernandes, M.J. Ramos, Molecular dynamics simulations of the amyloid-beta binding alcohol dehydrogenase (ABAD) enzyme, Bioorganic and Medicinal Chemistry 16 (2008) 9511–9518.

[52] R.P. Adhikari, R.P. Novick, Subinhibitory cerulenin inhibits staphylococcal exoprotein production by blocking transcription rather than by blocking secretion, Microbiology 151 (2005) 3059–3069.
[53] A.C. Price, Y.M. Zhang, C.O. Rock, S.W. White, Cofactor-induced conformational rearrangements establish a catalytically competent active site and a proton relay conduit in FabG, Structure 12 (2004) 417–428.
[54] J. Han, Q. Lu, L. Zhou, H. Liu, H. Xiang, Identification of the polyhydroxyalkanoate (PHA)-specific acetoacetyl coenzyme A reductase among multiple FabG paralogs in *Haloarcula hispanica* and reconstruction of the PHA biosynthetic pathway in *Haloferax volcanii*, Applied and Environment Microbiology 75 (2009) 6168–6175.
[55] S. Jenni, M. Leibundgut, D. Boehringer, C. Frick, B. Mikolasek, N. Ban, Structure of fungal fatty acid synthase and implications for iterative substrate shuttling, Science 316 (2007) 254–261.
[56] E. Habermann, K.L. Hardt, A sensitive and specific plate test for the quantitation of phospholipases, Analytical Biochemistry 50 (1972) 163–173.
[57] Z. Filip, S. Herrmann, J. Kubat, FT-IR spectroscopic characteristics of differently cultivated *Bacillus subtilis*, Microbiological Research 159 (2004) 257–262.
[58] R.J. Heath, S.W. White, C.O. Rock, Lipid biosynthesis as a target for antibacterial agents, Progress in Lipid Research 40 (2001) 467–497.